

ASTEROID ORBIT DETERMINATION FOR 5066 GARRADD 1990 MA

KARINA KRISHNAN, ELCIN KURNAZ, CHRIS REYES¹

¹*Summer Science Program*

(Dated: 10 July 2025)

ABSTRACT

This study consists applying Gauss' method to observational data collected from 5066 Garradd 1990 MA, a Mars-crossing asteroid, and comparing results with JPL reference values. We conducted observations over three nights at the Georgia College and State University Observatory. Images were calibrated using standard dark, flat, and light frames. Astrometric and photometric techniques were applied to extract accurate RA and Dec values of the asteroid, and these were used to compute position and velocity vectors via a Python implementation of Gauss's method. To verify the accuracy of our approach, we tested on known reference JPL data of our asteroid. Then we used the same method to compute six essential orbital elements for 5066 Garradd 1990 MA and compared to JPL values by using Monte Carlo simulations. The process is concluded with minimal percentage error, which displays the differences between the observational data and the exact values. Through the integration of classical orbit-determination techniques with modern observational data V. E. Savanevych et al. (2015), this work aims to elevate the understanding of 5066 Garradd 1990 MA and contribute to broader efforts in asteroid tracking and characterization, specifically based on 5066 Garradd 1990 MA.

1. INTRODUCTION

Precise calculation of the orbits of asteroids is necessary to advance scientific discovery. As more observations become available, data becomes more precise, and with the development of methods of orbital modeling, this field has accelerated. Studying asteroids provides critical insights into the discovery of the Solar System (B. Carry et al. (2016)). 5066 Garradd 1990 MA, is a Mars-crossing asteroid. Its orbit is .62 AU when it's closest to the Earth, consistent with Mars-crossing asteroids. Its eccentricity is quite high, with a value of approximately 0.4, and its period is approximately 3.2 years. 1990 MA has insufficient research done on it, making determining its orbit more significant. By following its orbit we can also understand similar Mars-crossing asteroids associated with 5066 Garradd 1990 MA. Asteroid determination gives us a greater understanding and allows us to detect any facial similarities in other Mars-crossing asteroids as well. Its proximity to Jupiter and Mars gives greater insight into the main belt's environment as well. Accurate orbit determination is essential for the understanding of the asteroid's past and future trajectory and risk potential. It can aid with planning future space missions as well (D. Perna et al. (2013); D. Perna et al. (2016)).

Recent research in asteroid orbit determination has focused on rotational properties and orbital dynamics

in characterizing small bodies. Investigations of Near-Earth Objects emphasize their significance in planetary defense (D. Perna et al. (2016)). Overall, these studies highlight the importance of precise observational data in redefining orbital and physical models (V. E. Savanevych et al. (2015)).

Mars-crossing asteroids lie in dynamically unstable regions between the main asteroid belt and near-Earth space that are influenced by planetary perturbations and resonances (M. Dellnitz et al. (2005)). They serve as key tracers of planetary migration and Solar System evolution (V. Alí-Lagoa & M. Delbo' (2017)). They have perihelia between 1.3-1.67 AU, making them particularly valuable for understanding the transport mechanisms that deliver material from the main belt to the inner Solar System (M. Dellnitz et al. (2005)). Current population studies estimate there are approximately 5,000 known Mars-crossers, representing about 4% of cataloged asteroids (V. Alí-Lagoa & M. Delbo' (2017))). Currently, our understanding of collision risks from Mars-crossing asteroids suggests they pose less immediate danger than NEOs, but their orbital evolution can lead them to become Earth-crossers over timescales of millions of years (M. Dellnitz et al. (2005)). The orbits of the asteroids that intersect Mars' orbit are likely to be of high eccentricity and will experience a dramatic change in their orbit with time. Eventually, their orbits have the

ability to evolve into Earth-crossing trajectories, which qualifies them as critical targets for monitoring and researching (D. Perna et al. (2013)). Ground-based observations remain of critical importance for population-level studies despite missions like Hayabusa2 (A. Fujiwara et al. (2006)) and OSIRIS-REx (D. S. Lauretta et al. (2017)) provided data on specific asteroids. Since the photographic plate era, the detection and characterization of Mars-crossing asteroids has evolved expansively. Modern surveys like WISE/NEOWISE have provided thermal infrared measurements of diameters and albedos for hundreds of Mars-crossers (V. Alí-Lagoa & M. Delbo' (2017)), and photometric studies have revealed their spin properties and potential binary nature (P. Pravec et al. (2016)). However, there still exist challenges in observing small or faint asteroids due to limited visibility time periods (V. E. Savanevych et al. (2015)). Their relatively small sizes (typically ≈ 10 km) and the gravitational perturbations from Mars that can significantly alter their trajectories (M. Dellnitz et al. (2005)), further underscoring the need for robust orbit-determination techniques.

2. METHODS

2.1. Target Selection

Asteroid 5066 Garradd 1990 MA is a valid target for this study due to its ability to be observed from the Georgia College and State University Observatory. This asteroid is categorized as a Mars-crossing asteroid, making the finding its orbit of importance. Additionally, it is of around 14V magnitude, making it bright enough for ideal visibility. GCSU is located in Milledgeville, Georgia, and has a latitude of $33^{\circ}51'N$. Garradd is well positioned at the GCSU observing site, as the elevation is well above 30 at each period of observation Ast (2025).

2.2. Observing Methods

We conducted our observation at GCSU with a 24-inch Corrected Dall-Kirkham (CDK 24) Astrograph telescope optical tube assembly manufactured by Planewave Instruments with focal ratio of f/6.8. We also received data from the Las Cumbres Observatory (LCO). One observation was taken from Cerro Tololo Inter-American Observatory with PROMPT 7 telescope with focal ratio of f/8 and another was taken at Siding Spring LCO Clamshell 2 which is a 2.3-meter telescope with the focal ratio of f/2.05. All standard procedures related to the base process for taking pictures of asteroids on the telescope were followed, including taking flats and darks in addition to science images.

To determine Asteroid 5066 Garradd 1990 MA's orbit, the method of Gauss was employed. Gauss' method

requires distance between image taking and intervals of observation. We observed for three nights taking 15 images with an exposure time of 1 minute and 15 seconds. These images were taken between ten minute intervals. These ten minute intervals occur to follow the asteroid's position throughout the night. Observing sessions were spaced out between a week of observations, to optimize the parallax effect necessary for orbit determination of 5066 Garradd 1990 MA via Gauss' method. To locate our asteroid we used JPL Horizons to obtain our RA and Dec for observing nights (as seen in table 1). All images were taken with a clear filter and 5-second exposure time.

DATES	RA	DEC
2025-06-23	15 30 23.75	-04 20 37.9
2025-06-29	15 21 25.62	-08 46 17.2
2025-07-08	15 11 29.10	-15 20 33.1

Table 1. Table of RA and DEC values from observation dates

2.3. Image calibration

We took a series of flats, darks, and lights on our telescope. On the days of our observations, we took a series of darks, and took a series of lights separated by three rounds with a ten-minute intermission.

2.4. Astrometry

To determine the RA and Dec of asteroid Garradd and to conduct centroiding, we determined an aperture around our asteroid, large, but not so large that other sources' interference would be included in the aperture. We also conducted background subtraction, so that the sky's brightness would not affect the centroid calculation. The object aperture we chose is 13 pixels, while the background is 20 pixels. Calibrated images were plate solved with Astronomer.net. Using the AstroImageJ software, 15 calibrated images from each set of images taken during one period were aligned, and stacked to focus the asteroid. After blinking the three sets of images from one observational period, the asteroid is identified, and the best set is chosen for photometry, leading to the estimation of the coordinates of asteroid Garradd.

2.5. Photometry

Using the software provided by SAO DS9 we input our data taken from the three nights using an aperture of 13 pixels with a background of 20 pixels. Doing the standard procedure in SAO gives us images with the ability to highlight stars. Once we transfer the image from SAO to AIJ we select five stars and go through

the standard imaging process. Selecting three radii, all four photometry icons, and doing linear regression to obtain a straight line fit. Afterwards, we use log10 of our asteroid, allowing the slope and y-intercept to become apparent, ultimately giving us our orbit.

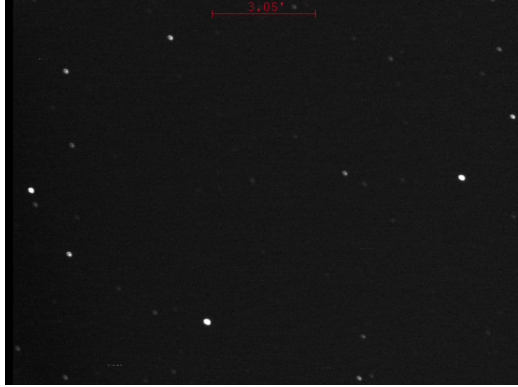


Figure 1. Image of 5066 Garradd 1990 MA

3. ORBIT DETERMINATION

3.1. Orbital Elements

There are six orbital elements that are necessary to understand and compute in order to perform Gauss' method. Once the position and vectors were determined, we calculated our 6 orbital elements.

The orbits of asteroids and anything that is heliocentric is elliptical. The equation of an ellipse is:

$$\frac{x^2}{a^2} + \frac{y^2}{b^2} = 1$$

Used to measure the size of an elliptical orbit, a is the semi-major axis in AU.

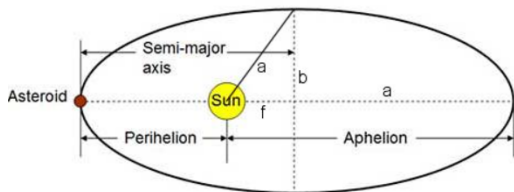


Figure 2. Figure of semi-major axis

^a<https://onlinehw.math.ksu.edu/math340book/capstone/kepler.php>

The elongation of an ellipse is described by e , or the eccentricity. A circular orbit has an e of 0, and a parabolic orbit has an e of 1. Therefore, it measures the amount by which the orbit deviates from a perfectly circular one.

The inclination (i) of an orbit is the angle between the orbital and the reference plane. For example, If the

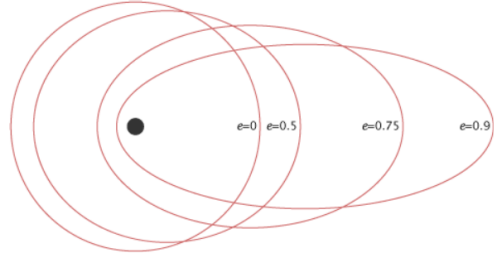


Figure 3. Visualization of different eccentricity values

^a<https://planetfacts.org/eccentric/>

inclination is zero, the object is in the other orbit under the reference plane. The value of 90 degrees stands for its polar orbit, whereas values between 90 and 180 cause move it to backwards. In Gauss's method, by measuring the angle that the angular momentum vector makes with the reference axis, the inclination can be computed by finding the arc cosine of the magnitude of the z-component of that vector.

Longitude of ascending node(Ω) is the angle between a fixed reference direction (usually the vernal equinox) and the point at which the orbit cuts the reference plane from south to north, called the ascending node. This angle defines the orientation of the orbited body with reference to this plane. It is always measured in the direction of the object's movement. After this angle is determined for the ascending node, it is used along with other orbital elements such as inclination, argument of periaxis, and eccentricity.

Argument of ascending node (ω): Argument of ascending node(ω) is where angle of the ascending node and point of periaxis(closest approach) is found. This is always measured in the direction of the object's motion. Periaxis and apoapsis refer to the objects nearest and farthest approach in their orbits. It crosses the equatorial plane. You determine the angle of the object's orbit, use the longitude of the ascending node, and afterwards consider other major orbits such as the semi-major axis eccentricity, and mean anomaly to determine a body's position in orbit.

Mean anomaly (M) is the fraction of an elliptical orbit that has elapsed since it passed periaxis. Expressed as an angle, we use it to calculate an orbiting body in a two-body problem. It also represents the angle between the lines drawn from the sun to perihelion. We use it for asteroid orbit T (time it takes for one period) t_0 for when the asteroid was closest to our sun, and this gives us the anomaly.

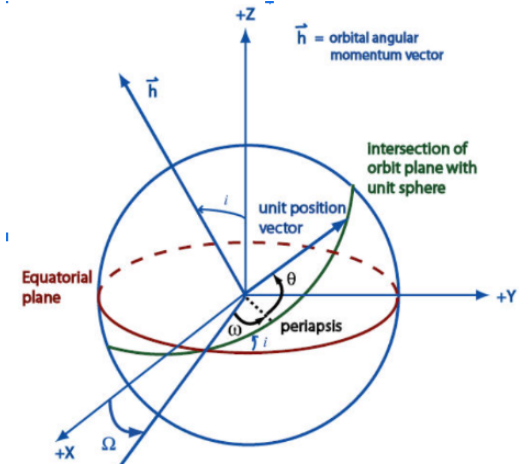


Figure 4. Diagram of 3 orbital elements: Ω is the argument of periapsis, i is the true anomaly, and ω is the right ascension of the ascending node

a https://help.agi.com/STKComponents/html/PAGI_Foundation_Coordinates_KeplerianElements_Inclination.htm

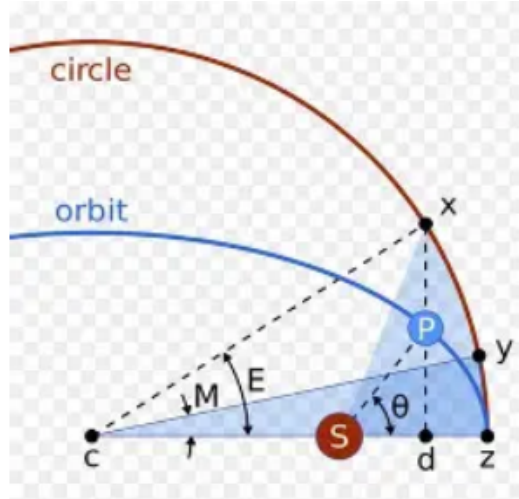


Figure 6. A diagram showing mean and eccentric anomaly.

a https://commons.wikimedia.org/wiki/File:Mean_Anomaly.svg

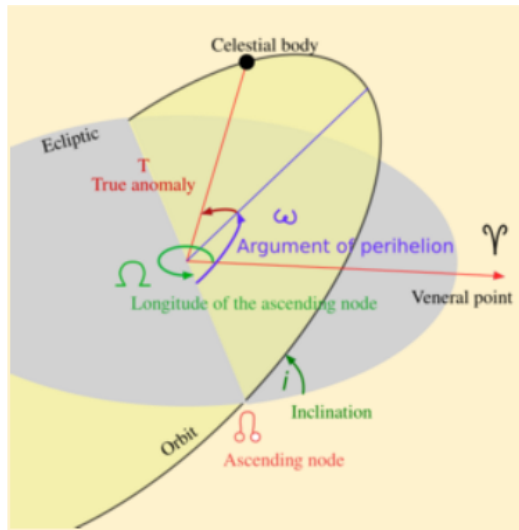


Figure 5. 6 orbital elements

a <https://www.astronomicalreturns.com/p/section-43-six-orbital-elements.html>

3.2. Method of Gauss

Precise observational data and mathematical techniques are required to generate an orbital description. First, position and velocity are calculated using three observations of the asteroid's Right Ascension (RA) and Declination (Dec) and applying the Method of Gauss at a reference time. Then, the six orbital elements, introduced earlier, that define an asteroid's trajectory are calculated. The sun's position vectors are generated from JPL Horizons at observation times. This struc-

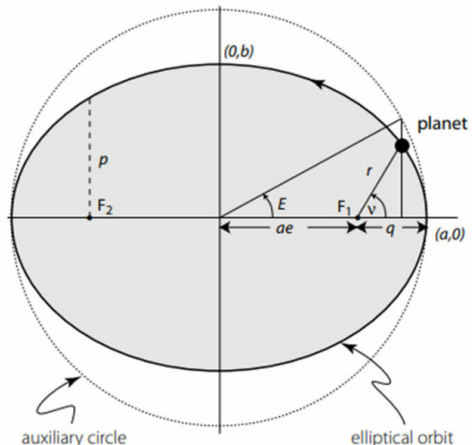


Figure 7. The Eccentric anomaly and the true anomaly. The mean anomaly is defined as the angle the planet would travel (in the same time) on the ellipse's auxiliary circle.

a <https://www.researchgate.net/figure/The-Eccentric-anomaly-and-the-true-anomaly-The-mean-anomaly-is-defined-as-the-angle-the-figure2369057893>

tured methodology allows for the determination of 5066 Garradd 1990 MA's orbit, enabling further dynamical studies and ephemeris predictions. To determine the orbit of asteroid 5066 Garradd 1990 MA, the Method of Gauss was employed, which allows us to compute the position and velocity vectors of the asteroid from three observational data points. The first step is documenting the RA and Dec of the asteroid at three distinct observation times, (t_1, t_2, t_3), along with the corresponding

heliocentric position vectors of the Sun at these times,

$$(\hat{R}_1, \hat{R}_2, \hat{R}_3)$$

. The RA and Dec were converted into decimal degrees for coding purposes.

Using the observed RA and Dec, we computed the unit vectors, $\hat{\rho}_1, \hat{\rho}_2, \hat{\rho}_3$ for each observation:

$$\hat{\rho}_i = \begin{bmatrix} \cos \alpha_i \cos \delta_i \\ \sin \alpha_i \cos \delta_i \\ \sin \delta_i \end{bmatrix}$$

The time intervals between observations were converted into Gaussian time units:

$$\tau_1 = k(t_1 - t_2), \tau_3 = k(t_3 - t_2), \tau_2 = k(t_3 - t_1) \quad (1)$$

k is the Gaussian gravitational constant.

Initial values for the coefficients a_1 and a_3 were calculated as:

$$\begin{aligned} a_1 &= \frac{\tau_3}{\tau_2} \\ a_3 &= -\frac{\tau_1}{\tau_2} \end{aligned} \quad (2)$$

These coefficients were used to estimate the geocentric distances ρ_1, ρ_2, ρ_3 through scalar triple products involving \vec{R}_i and $\hat{\rho}_i$.

$$\rho_n = \frac{a_1 D_{n1} - D_{n2} + a_3 D_{n3}}{a_n D_0}$$

The initial position vectors r_i were computed as:

$$r_i = \rho_i * \hat{\rho}_i - R_i \quad (3)$$

The velocity vector v_2 at the middle observation time t_2 was approximated:

$$\vec{v}_2 = \frac{(t_3 - t_2)\vec{v}_{12} + (t_2 - t_1)\vec{v}_{23}}{(t_3 - t_1)} \quad (4)$$

\vec{v}_{12} and \vec{v}_{23} are the velocities between the respective observation pairs.

$$\vec{v}_{12} = \frac{\vec{r}_2 - \vec{r}_1}{t_2 - t_1}, \vec{v}_{23} = \frac{\vec{r}_3 - \vec{r}_2}{t_3 - t_2}$$

Starting with the initial estimates of a_1 and a_3 , we iteratively refined the values of a_1, a_3, ρ_i, r_i , and v_2 by solving the system of equations involving the f and g Taylor Series expansions:

$$f(\tau) = [1 - \frac{\tau^2}{2r_2^3} + \frac{(\vec{r}_2 \cdot \dot{\vec{r}}_2)\tau^3}{2r_2^5} + \frac{\tau^4}{24r_2^3}(3(\frac{\vec{r}_2 \cdot \dot{\vec{r}}_2}{2r_2^5} - \frac{1}{r_2^3}) - 15(\frac{\vec{r}_2 \cdot \dot{\vec{r}}_2}{r_2^2})^2 + \frac{1}{r_2^3})] \quad (5)$$

$$g(\tau) = [\tau - \frac{\tau^3}{6r_2^3} + \frac{(\vec{r}_2 \cdot \dot{\vec{r}}_2)\tau^4}{4r_2^5}] \quad (6)$$

$$f_1 = f(\tau_1), g_1 = g(\tau_1), f_3 = f(\tau_3), g_3 = g(\tau_3)$$

where a_1 and a_3 is:

$$a_1 = \frac{g_3}{f_1 g_3 - f_3 g_1}, a_3 = \frac{g_1}{f_1 g_3 - f_3 g_1}$$

The loop is iterated through until the position vector converged to a tolerance of 10^{-10} .

To account for the finite speed of light, we adjusted the observation times and recomputed the position and velocity vectors, ensuring higher accuracy.

Finally, using rotational matrices, the refined position and velocity vectors were transformed from the equatorial coordinate system to the ecliptic coordinate system, preparing them for orbital element calculation.

3.3. Orbital element calculation

We computed the six classical orbital elements to fully describe the orbit of 5066 Garradd 1990 MA:

Semi-major axis (a): a is calculated using the specific orbital energy: $(a = \frac{1}{\frac{2}{r_2} - \frac{v_2^2}{\mu}} \mu)$ is the standard gravitational parameter, which we set to 1 for all calculations.

Eccentricity (e):

Derived from the angular momentum:

$$h_{vector} = \vec{r}_2 \cdot \vec{v}_2,$$

and energy:

$$e = \sqrt{1 - \frac{h^2}{\mu a}}$$

Inclination (i): The angle between the orbital plane and the ecliptic plane, found using: $\cos i = \frac{h_z}{h_{mag}}$

Longitude of the Ascending Node (Ω): The angle from the vernal equinox to the ascending node, determined by:

$$\tan(\Omega) = -\frac{Nx}{Ny}$$

$$N = k_{hat} \cdot h$$

Argument of Perihelion (ω): The angle from the ascending node to the perihelion, calculated using the eccentricity vector:

$$\cos(\omega) = \frac{Ne}{N_{mag} \cdot e_{mag}}$$

True anomaly (ν): The angle between the perihelion and the asteroid's current position, given by:

$$\cos(\nu) = \frac{e \cdot r_2}{e_{mag} \cdot r_{2mag}}$$

All of these essential orbital components define the size, shape, and orientation of the 5066 Garradd 1990 MA orbit. This enables us to predict its future trajectory and position in the solar system.

3.4. Uncertainty estimation method

To calculate the orbital elements, our group used Visual Studio Code to calculate the semi-major axis, eccentricity, inclination, longitude of ascending node, argument of perihelion, and mean anomaly. We first used practice data from JPL, which was asteroid 2002 QF15 00:00:00 UT on July 14th, 2018; expecting a 0.02 % error or less using the method of Gauss. We used f and g formulas from the Gauss equations.

$$f(\tau) = [1 - \frac{\tau^2}{2r_2^3} + \frac{(\vec{r}_2 \cdot \dot{\vec{r}}_2)\tau^3}{2r_2^5} + \frac{\tau^4}{24r_2^3} (3(\frac{\vec{r}_2 \cdot \dot{\vec{r}}_2}{2r_2^5} - \frac{1}{r_2^3}) - 15(\frac{\vec{r}_2 \cdot \dot{\vec{r}}_2}{r_2^2})^2 + \frac{1}{r_2^2})] \quad (7)$$

$$g(\tau) = [\tau - \frac{\tau^3}{6r_2^3} + \frac{(\vec{r}_2 \cdot \dot{\vec{r}}_2)\tau^4}{4r_2^5}] \quad (8)$$

We ran these equations through Monte Carlo simulations to get the lowest possible error. Getting it lower or close to 0.02% error. After running the practice, we then used our own data from 5066 Garradd 1990 MA and input our given values into the orbit determination (OD).

3.5. Orbital elements results

In the table, we placed the six orbital elements which we calculated from our Python code. Calculated values for 6 orbital elements are in the first column and references values are in the second column. Finally, we define the error percentage and standard deviation between the specific day values and the reference data.

Also, we determined the histograms for the distribution of 6 orbital elements' values:

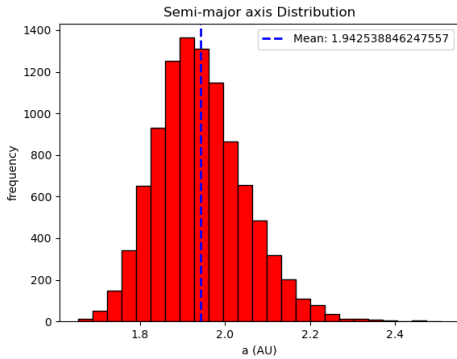


Figure 8. Histogram for distribution of semi-major axis values: mean of a is 1.94
standard deviation of mean of error of a is 0.17

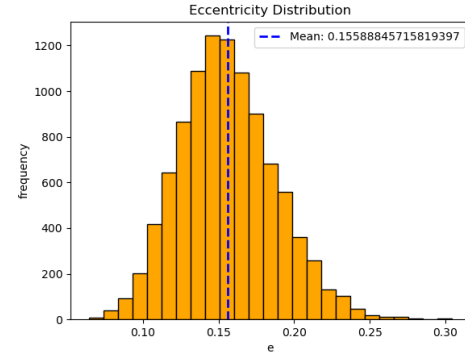


Figure 9. Histogram for distribution of eccentricity values:
mean of e is 0.15
standard deviation of mean of error of e is 2.17

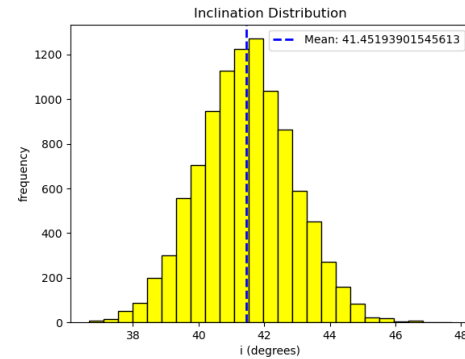


Figure 10. Histogram for distribution of inclination values:
mean of i is 41.40
standard deviation of mean of error of i is 0.01

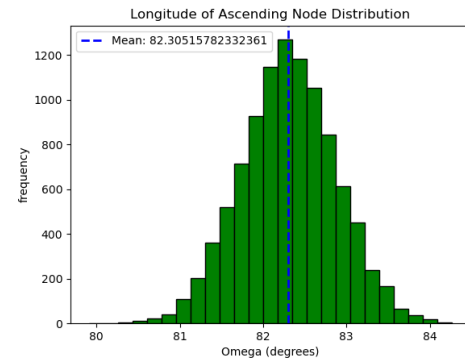


Figure 11. Histogram for distribution of longitude of ascending node values: mean of Ω is 82.33
standard deviation of mean of error of Ω is 0.004

4. CONCLUSION AND DISCUSSION

In conclusion, after the Gauss' method's steps and error interpretation for orbital elements, we concluded our uncertainty values. We calculated the error per-

Element	Calculated	References	Error Percentage	Standard Deviation
a	1.96	1.94	0.99	0.10
e	0.16	0.15	2.53	0.03
i	41.861	41.46	0.97	1.43
Ω	82.14	82.28	0.17	0.57
ω	182.44	184.82	1.29	5.71
M	353.45	351.68	0.50	30.05

Table 2. Orbital elements data of observation dates and reference values from JPL

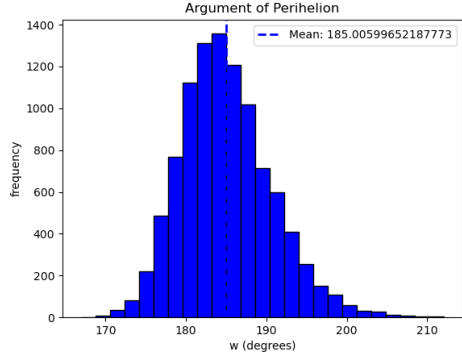


Figure 12. Histogram for distribution of argument of perihelion values: mean of ω is 185.19
standard deviation of mean of error of ω is 0.002

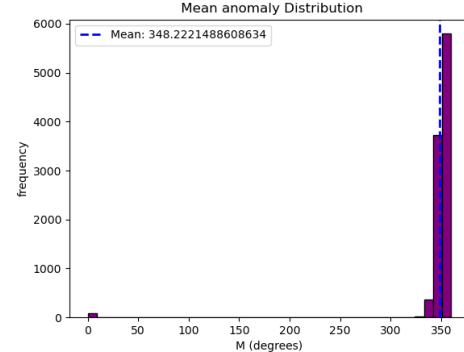


Figure 13. Histogram for distribution of mean anomaly values: mean of M is 348.65
standard deviation of mean of error of M is 0.001

centage and the standard deviation, which are shown in table 2. These error values are 0.17% between 2.53%, which displays the similarity and consistency of our values compared to the actual reference JPL values. While we conducted our observational process and data reduction steps carefully, some sources of uncertainty still exist, even in ideal conditions. The primary issue is the limitation on astrometric precision due to atmospheric distortion and seeing conditions. Even small errors in determining the asteroid's RA and Dec can grow significantly through Gauss's method.

Another significant source of error comes from the time gaps and spacing between our observation dates. We picked three nights that were spaced nearly 1 week apart. However, uneven sky conditions, minor errors in timing or positioning of the observations and since our asteroid is a moon-crossing asteroid, the angle between our asteroid and the moon can lead to compounded mistakes in measuring the velocity and the position vectors. These problems might explain the differences we see between our calculated orbital elements and the reference values from JPL. Future work could improve this approach by increasing the number of observation nights to allow for stronger orbit fitting and error estimation. It is unlikely that the asteroid has changed course, but our comparison with JPL's data offers a useful reference for understanding the limits of our asteroid .

REFERENCES

2025, Asteroid+Garradd— Space Reference, Space Reference.
<https://www.spacerefERENCE.org/asteroid/5066-garradd-1990-ma>

Alf-Lagoa, V., & Delbo', M. 2017, Astronomy amp; Astrophysics, 603, A55,
doi: [10.1051/0004-6361/201629917](https://doi.org/10.1051/0004-6361/201629917)
Carry, B., Solano, E., Eggl, S., & DeMeo, F. E. 2016,
Icarus, 268, 340, doi: [10.1016/j.icarus.2015.12.047](https://doi.org/10.1016/j.icarus.2015.12.047)

- Dellnitz, M., Junge, O., Lo, M. W., et al. 2005, PhRvL, 94, 231102, doi: [10.1103/PhysRevLett.94.231102](https://doi.org/10.1103/PhysRevLett.94.231102)
- Fujiwara, A., Kawaguchi, J., Yeomans, D. K., et al. 2006, Science, 312, 1330, doi: [10.1126/science.1125841](https://doi.org/10.1126/science.1125841)
- Lauretta, D. S., Balram-Knutson, S. S., Beshore, E., et al. 2017, SSRv, 212, 925, doi: [10.1007/s11214-017-0405-1](https://doi.org/10.1007/s11214-017-0405-1)
- Perna, D., Barucci, M. A., & Fulchignoni, M. 2013, A&A Rv, 21, 65, doi: [10.1007/s00159-013-0065-4](https://doi.org/10.1007/s00159-013-0065-4)
- Perna, D., Dotto, E., Ieva, S., et al. 2016, AJ, 151, 11, doi: [10.3847/0004-6256/151/1/11](https://doi.org/10.3847/0004-6256/151/1/11)
- Pravec, P., Scheirich, P., Kušnírák, P., et al. 2016, Icarus, 267, 267, doi: [10.1016/j.icarus.2015.12.019](https://doi.org/10.1016/j.icarus.2015.12.019)
- Savanevych, V. E., Briukhovetskyi, O. B., Sokovikova, N. S., et al. 2015, MNRAS, 451, 3287, doi: [10.1093/mnras/stv1124](https://doi.org/10.1093/mnras/stv1124)